Vol. 88: 61–79, 2022
https://doi.org/10.3354/ame01982

AQUATIC MICROBIAL ECOLOGY
Aquat Microb Ecol

Published online February 24

Microbial communities (bacteria, archaea and eukaryotes) in a temperate estuary during seasonal hypoxia

Luciana F. Santoferrara[1,2,5,*], George B. McManus[2], Dianne I. Greenfield[3,4], Susan A. Smith[2]

[1]Department of Ecology and Evolutionary Biology, University of Connecticut, Storrs, CT 06269, USA
[2]Department of Marine Sciences, University of Connecticut, Groton, CT 06340, USA
[3]Advanced Science Research Center at the Graduate Center, City University of New York, New York, NY 10031, USA
[4]School of Earth and Environmental Sciences, Queens College, Flushing, NY 11367, USA

[5]*Present address:* Department of Biology, Hofstra University, Hempstead, NY 11549, USA

ABSTRACT: Eutrophication and hypoxia markedly alter trophic dynamics and nutrient cycling in estuarine water columns, but little is known about the microbial communities that drive and interact with these changes. Here we studied microbial plankton (bacteria, archaea, protists and micro-metazoans) in a large temperate estuary where bottom hypoxia occurs every summer due to warmer temperatures, stratification, and oxidation of organic matter fueled by nutrient enrichment. We used high-throughput sequencing of the 16S and 18S rRNA genes (V4 region) and quantified multiple abiotic and biotic factors in surface and bottom waters during the summer of 2019. The conditions associated with the intensification of hypoxia in bottom waters as the summer progressed were linked to significant changes in the diversity, community structure and potential functioning of microbial communities. Under maximum hypoxia (dissolved oxygen concentration: 0.9–3.1 mg l^{-1}), there were increased proportions of ammonia-oxidizing archaea (AOA), bacterivorous and parasitic protists, and copepod nauplii. Sequence proportions of AOA (*Nitrosopumilus*) and nitrite-oxidizing bacteria (*Nitrospinaceae*) were significantly correlated with the concentration of oxidized N species (nitrite plus nitrate, which peaked at 14.4 µM) and the proportions of nauplii DNA sequences and biomass. Our data support a tight coupling of biogeochemical and food web processes, with rapid oxidation of ammonia and accumulation of oxidized N species as hypoxia intensifies during the summer.

KEY WORDS: Microbial plankton · Prokaryotes · Protists · DNA · Deoxygenation · Eutrophication · Long Island Sound

1. INTRODUCTION

Globally, marine ecosystems are experiencing interacting stressor conditions, including warming, acidification and deoxygenation (Gobler & Baumann 2016, Breitburg et al. 2018). Low or no dissolved oxygen (DO) in the water (hypoxia or anoxia, respectively) results from natural processes in the 'oxygen minimum zones' (OMZs) that occur in western continental margins with persistent nutrient-rich upwelling (Helly & Levin 2004, Stramma et al. 2008) or in a variety of systems such as semi-enclosed seas, river-dominated shelves, fjords and hydrodynamically constrained estuaries (Fennel & Testa 2019). An additional cause for oxygen loss in coastal areas is anthropogenic nutrient enrichment, which has mag-

*Corresponding author: luciana.santoferrara@hofstra.edu

nified deoxygenation in the past 60 yr (Diaz & Rosenberg 2008, Zhang et al. 2010). Deoxygenation is also intensified globally by climate change, mainly because warming decreases both oxygen solubility and the ventilation of the water column due to intensified stratification (Altieri & Gedan 2015, Schmidtko et al. 2017, Breitburg et al. 2018). On the other hand, coastal hypoxia stimulates water and sediment biogeochemical processes that release powerful greenhouse gases (nitrous oxide and methane), potentially leading to positive feedbacks on climate change (Naqvi et al. 2010, Voss et al. 2013).

In estuaries, hypoxia (and in some cases anoxia) can result from the combined effects of nitrogen pollution from agriculture, urbanization and atmospheric deposition, as well as geological and climatic factors that influence residence times, vertical mixing and re-oxygenation of bottom waters (Hagy et al. 2004, Howarth et al. 2011, Fennel & Testa 2019). In temperate eutrophic estuaries, hypoxia occurs in summer, when stratification provides the best light conditions for primary production above the pycnocline, while it limits the re-oxygenation of bottom waters. Increased N loads fuel phytoplankton growth, with excess cells settling and being decomposed by microbial activities that consume DO. If DO demands by pelagic and benthic processes exceed re-oxygenation of bottom waters by photosynthesis and/or mixing, hypoxia occurs (Crump et al. 2007).

Hypoxia thresholds are defined at DO concentrations between 2 and 4.6 mg l^{-1}, with values being adjusted based on key negative outcomes in different systems (Steckbauer et al. 2011, Breitburg et al. 2018). The most well-known biological effect of hypoxia is the episodic mortality, sometimes massive, of fish and benthic invertebrates (Vaquer-Sunyer & Duarte 2008, Breitburg et al. 2009). In these 'dead zones' for macroorganisms, recurrence of severe events and chronic exposure to mild hypoxia can prevent full population recovery, chronically displace organisms towards more oxygenated waters, and cause progressive deterioration of fisheries and overall ecosystem functioning (Breitburg et al. 2009, Steckbauer et al. 2011). Studies on the relationship between hypoxia and the structure of pelagic food webs have focused on primary producers and top consumers, with reports of reduced energy transfer under hypoxia (Baird et al. 2004). As important trophic links, mesozooplankton have been considered in hypoxia research (Keister & Tuttle 2013, Hauss et al. 2016, Seibel et al. 2016, Ekau et al. 2010), and effects that range from mortality to prey avoidance are documented for copepods (Marcus et al. 2004, Ludsin et al. 2009, Elliott et al. 2013). Much less is known about the influence of deoxygenation on smaller plankton.

Microbial communities form the base of aquatic food webs and drive major biogeochemical cycles, thus playing crucial roles in the environment. Major changes in microbial community structure and function are expected as a consequence of ocean warming, acidification and deoxygenation, but many gaps in the knowledge remain and multiple interactive factors make it difficult to predict net outcomes (Caron & Hutchins 2013, Hutchins & Fu 2017, Cavicchioli et al. 2019). Most of what is known on the reationships between DO variations and microbial plankton is from naturally occurring OMZs and anoxic basins, where the sharpest community variations correlate with changes in redox potential across the water column (e.g. Stoeck et al. 2010, Edgcomb et al. 2011, Wright et al. 2012, Bertagnolli & Stewart 2018, Torres-Beltrán et al. 2018, De La Iglesia et al. 2020). However, changes in microbial communities and feedbacks with trophic and biogeochemical dynamics likely differ in coastal systems where hypoxia is seasonal, is highly influenced by cultural eutrophication, and develops in shallow water columns tightly coupled to benthos and sediment. Known effects of coastal eutrophication on microbial plankton include shifts in phytoplankton composition from diatom to dinoflagellate and nanoflagellate dominance, as well as a higher prevalence of harmful algal blooms (Kemp et al. 2005, Verity & Borkman 2010, López Abbate et al. 2015, Reed et al. 2016) and increased proportions of bacterivorous protists and bacterivory rates (Stauffer et al. 2013, Tadonléké et al. 2016). In parallel, prokaryotic metabolism progressively switches from the oxygen-requiring processes that lead to hypoxia (aerobic respiration, nitrification) to anaerobic reductive processes such as denitrification, methanogenesis and sulfate reduction (Baird et al. 2004, Crump et al. 2007, Rabouille et al. 2008, Hewson et al. 2014). Still, the complexity of biological and abiotic processes in diverse coastal ecosystems, especially in estuaries, makes it difficult to elucidate the relationships between hypoxia and microbial plankton communities.

Prokaryotic and eukaryotic communities are tightly interconnected by trophic interactions, energy flux and nutrient recycling in the microbial food web, but both components have rarely been studied concurrently in seasonally hypoxic estuaries. In one of the few examples, a metatranscriptome analysis of microbial communities (0.2–64 µm) in the Chesapeake Bay

estuary (Northeast USA) indicated potential taxonomic and functional shifts with depth and from spring to late summer, with higher expression of photoautotrophy genes in surface waters versus genes involved in respiration, DNA recycling and regulation in deep oxic and anoxic waters (Hewson et al. 2014). In the present paper, we study another large temperate estuary of the Northeast USA, Long Island Sound (LIS), which consistently experiences eutrophication and summer hypoxia (Anderson & Taylor 2001, Capriulo et al. 2002). We simultaneously assessed changes in community structure based on the V4 region of the 16S and 18S rRNA genes to characterize the diversity and taxonomic composition of bacteria, archaea and microbial eukaryotes before and during maximum hypoxia. We also generated metagenome predictions based on bacterial and archaeal sequences (Douglas et al. 2020) to evaluate potential functional shifts in relation to environmental conditions. We hypothesized that, in parallel to hypoxia intensification, there are significant changes in (1) the microbial community structure, with a switch from bacterial to archaeal prevalence, and from phytoplankton and grazers (e.g. copepod nauplii) to bacterivore protists, and (2) the genetic potential for oxygen-sensitive processes, such as nitrogen-cycling reactions.

2. MATERIALS AND METHODS

2.1. Study area

LIS is a 3400 km^2, semi-enclosed estuary surrounded by New York City and its metropolitan area in the west and the suburban areas of Long Island and Connecticut in the east (Fig. 1A). It is narrower on its western boundary with the East River, where it is also most impacted by urban wastewaters, and wider on its east boundary with the Atlantic Ocean. The discharges of several rivers define the circulation, with fresher surface waters leaving the Sound and saline bottom waters flowing in (Wilson et al. 2008). This circulation pattern, along with seasonal warming, contributes to weak but persistent summer stratification. Due to both nutrient enrichment and stratification, the 20–40 m deep, westernmost section of LIS (the Narrows, or WLIS) experiences hypoxia in the bottom 10–20 m of the water column every summer (Wilson et al. 2008, Gobler & Baumann 2016).

Despite improvements in wastewater treatment processes that have led to measurable shrinkage in the area and volume of hypoxic water (Whitney & Vlahos 2021), seasonal hypoxia persists in WLIS. The

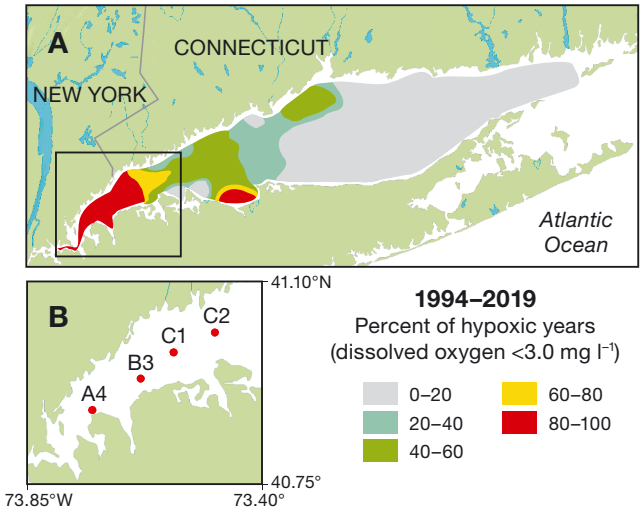

Fig. 1. Long Island Sound. (A) Distribution of hypoxia from 1994 to 2019 (data from the Connecticut Department of Energy and Environmental Protection). (B) Stations sampled for the present study

Connecticut Department of Energy and Environmental Protection (CT DEEP) has reported hypoxia, defined as DO levels below 3 mg l^{-1}, in areas that varied from 80 to 1020 km^2 during the last 25 summers (Fig. 1A; CT DEEP 2020). For the present study, we collected samples along with the CT DEEP Water Quality Monitoring Program in summer 2019. During that year, the hypoxic area reached 230 km^2; it started to develop during the second half of July, had maximum intensity during the first half of August and dissipated by the beginning of September (CT DEEP 2020).

2.2. Sampling and quantification of environmental parameters

Sampling was conducted on board the R/V 'Dempsey' in WLIS at the onset of hypoxia (July 15) and during maximum hypoxia (August 12) in 2019 (Fig. 1B, Table S1 in the Supplement at www.int-res.com/articles/suppl/a088p061_supp.xlsx). At each station, water clarity was measured with a Secchi disk, and vertical profiles of salinity, temperature, pH and DO were measured with a conductivity, temperature, depth instrument (CTD) mounted on a rosette. Niskin bottles were used to collect water at 2 depths, defined as 'surface' (2 m below surface) and 'bottom' (5 m above bottom).

For quantification of dissolved inorganic nutrients (nitrate plus nitrite = NO_x^-, ammonium = NH_4^+ and orthophosphate = PO_4^{3-}; Stns A4 and C1 only), water samples were collected in triplicate in 1 l Nalgene bot-

tles, then filtered through 0.7 µm pore-size glass fiber (GF/F) filters (Whatman). These and all other filtrations mentioned below were done under gentle (5 mm Hg) vacuum. Filtrate from each replicate was collected in scintillation vials, frozen (–20°C), then analyzed colorimetrically within 28 d using a Lachat 8500+ series autoanalyzer following standard methods (Zimmerman & Keefe 1991, Grasshoff et al. 1999). Water samples were also filtered on to GF/F filters and stored in the dark at –20°C until fluorometric quantification of chlorophyll *a* (chl *a*) concentration as a proxy of phytoplankton biomass (Welschmeyer 1994).

For quantification of microzooplankton biomass (primarily heterotrophs 20–200 µm long), 0.5 l samples were preserved with non-acid Lugol's solution (2% final concentration). The whole volume was then settled down for counting and measuring ciliates, dinoflagellates, copepod nauplii (larger stages up to 450 µm long were also included) and rotifers in an inverted microscope. Volume conversion factors were applied to estimate carbon content for protists, and a length-based regression was used for micrometazoans (Putt & Stoecker 1989, Lessard 1991, Godhantaraman & Uye 2003).

For DNA sequencing, 0.5 l samples were carefully pre-screened through a 200 µm mesh to remove large organisms, then filtered sequentially through 2 and 0.2 µm pore-size polycarbonate membrane filters (Millipore). To prevent cross-contamination among samples, filtration columns were pre-rinsed at least 3 times with sample water. At the end of the sampling on July 15, a negative control was generated by sequentially passing sterile water through the filtration columns and then a 0.2 µm filter. All filters were placed in sterile lysis buffer (100 mM NaCl, 0.5% SDS, Tris–EDTA at pH 8) and stored at –20°C until DNA extraction.

2.3. DNA extraction, PCR amplification and sequencing

DNA was extracted with the Fecal/Soil Microbiome kit D6012 (Zymo Research). An additional negative control (lysis buffer) was generated to check for contamination during laboratory procedures. DNA samples were quantified with the Qubit DNA broad range assay (Life Technologies).

For DNA extracted from 0.2 or 2 µm filters, the V4 region of the 16S or 18S rRNA gene (referred to as 16S or 18S from here onwards) was amplified with the primers 515F–806R (Apprill et al. 2015, Parada et al. 2016) or TAReuk454FWD1–TAReukREV3 (Stoeck et al. 2010), respectively. The 16S primers were customized for Illumina dual indexing of amplicons in a single PCR step (Kozich et al. 2013). The 18S primers included an overhang, and a second PCR was needed for dual indexing (Lange et al. 2014). Reactions included 10 ng of DNA and the following reagents (Promega GoTaq® PCR Core Systems): 5.0 µl 5X buffer, 2.5 µl $MgCl_2$, 0.7 µl dNTPs (10 mM), 0.25 µl *Taq* polymerase, and 1 µl of each primer (10 µM). For 16S, PCR conditions were: 95°C for 3.5 min, 30 cycles of 95°C for 30 s, 50°C for 30 s and 72°C for 90 s, and final extension at 72°C for 10 min. For 18S, conditions for the first PCR were: 95°C for 2 min, 10 cycles of 95°C for 10 s, 53°C for 30 s and 72°C for 30 s, followed by 15 cycles of 95°C for 10 s, 48°C for 30 s and 72°C for 30 s, and final extension at 72°C for 2 min; and for the second PCR: 95°C for 3.5 min, 8 cycles of 95°C for 30 s, 50°C for 30 s and 72°C for 90 s, and final extension at 72°C for 10 min.

Triplicate PCR products per sample were pooled before quantification and visualization with QIAxcel DNA Fast Analysis (Qiagen). Pools were normalized based on expected amplicon length and DNA concentration, then combined with the QIAgility liquid handling robot, and cleaned with the Gene Read Size Selection kit (Qiagen). Paired-end sequencing was done in a single run with the MiSeq instrument and the 2x250 base pair kit v. 2 (Illumina) at the Microbial Analysis, Resources and Services (MARS) facility, University of Connecticut. The filtering and extraction controls were amplified with both primer sets and sequenced along with the samples. These negative controls yielded a negligible number of reads and sequence compositions significantly different from the samples (Table S1). The ZymoBIOMICS Microbial Community DNA Standard D6305/D6306 (Zymo Research) was amplified with the 16S primer set, sequenced, and checked for the expected even distribution of amplicon relative abundances. Sequencing failed for 3 samples (Table S1).

2.4. Bioinformatic and statistical analyses

The 16S and 18S raw datasets are available in the NCBI Sequence Read Archive (accession number: PRJNA770032). Sequences were demultiplexed and quality-filtered in BaseSpace (Illumina). Subsequent processing was done in QIIME 2 (Bolyen et al. 2019). After primer trimming with the cutadapt plugin (Martin 2011), sequence quality was evaluated to select parameters for the next step. Denoising, dereplication and chimera removal were done with DADA2 (Calla-

han et al. 2016). Taxonomic classification of amplicon sequence variants (ASVs) used a naive Bayes classifier (Pedregosa et al. 2011) trained on V4-trimmed versions of SILVA v. 132 for 16S (Quast et al. 2013) and PR^2 v. 4.12 for 18S (Guillou et al. 2013; ranks above phylum were updated based on Adl et al. 2019 and Burki et al. 2020). ASVs annotated as chloroplast or mitochondrion sequences were eliminated.

Annotation of functional potential based on the 16S ASVs was done with PICRUSt2 (Douglas et al. 2020). This method generates metagenome predictions based on phylogenetic placement of 16S rRNA gene sequences in a reference framework of bacterial and archaeal genomes. Functional predictions based on Enzyme Commission numbers (ECs), KEGG orthologs (KOs) and MetaCyc metabolic pathways (MPs) were done under default conditions with a nearest-sequenced taxon index cut-off of 2 (Douglas et al. 2020). Differences in the relative contribution of KOs and MPs between sample groups were estimated as the $\log_2$ of fold-changes, and KOs of interest were mapped with KEGG Mapper (Kanehisa & Sato 2020). Although PICRUSt2 or similar methods are not available for eukaryotic microbes, taxonomy and function are well correlated in protists (Ramond et al. 2019). Thus, functional assumptions for protists were based on taxonomy (Adl et al. 2019, Burki et al. 2020).

Multivariate and statistical analyses were done in QIIME2 (Bolyen et al. 2019) and in R v. 3.6.3 (R Core Team 2020) using the *vegan* package (Oksanen et al. 2019). Sequence data were rarefied to the minimum sampling depth. Environmental data were standardized to scale each variable to a zero mean and unit variance. Alpha-diversity was computed as observed ASV richness and Shannon index, and differences between sampling depths and periods were tested with pairwise *t*-tests. Beta-diversity was evaluated with principal coordinates analyses (PCoA) computed with qualitative (Jaccard, unweighted Unifrac) and semi-quantitative (Bray-Curtis, weighted Unifrac) index matrices; because all metrics yielded comparable outputs, only the Bray-Curtis results are shown. PCoAs were also computed with Bray-Curtis matrices based on PICRUSt2 outputs (ECs, KOs and MPs); because the 3 ordinations were almost identical, only the MP results are shown. The significance of sample groups was evaluated with ANOSIM using 999 permutations (Clarke 1993). Pairwise correlations between selected variables were tested with Pearson's coefficient (R). The correlation between Bray-Curtis dissimilarity (sequence) and Euclidean distance (environmental) matrices was tested with the Mantel test using 999 permutations (Legendre & Legendre 2012). The subsets of environmental variables that best correlated with sequence-based beta-diversity were identified with BIO-ENV (Clarke & Ainsworth 1993).

3. RESULTS

3.1. General abiotic and biotic factors

We studied WLIS waters at the onset of hypoxia (July) and during maximum hypoxia (August) (Table S1, Fig. 2). Temperature and salinity ranged from 17.0 to 23.3°C and 23.3 to 27.6, respectively. Vertical profiles show the typical summer stratification that limits vertical mixing (Fig. 2A,B), thus favoring lower DO in bottom waters (Fig. 2C). DO ranged from 4.6 to 9.4 mg l^{-1} in surface waters during both periods. In bottom waters, this parameter ranged from 4.1 to 4.8 mg l^{-1} in July, except for a value of 2.5 mg l^{-1} in the westmost station. In August, bottom waters were hypoxic or borderline hypoxic in all sampled stations (0.9–3.1 mg l^{-1}), with the westmost station showing the minimum DO recorded in 2019 (CT DEEP 2020).

Among the inorganic nutrients quantified, NO_x^- showed the most variable values, with concentrations <0.1 µM in July surface waters and up to 14.4 µM in August bottom waters. The concentrations of NH_4^+ (0.1–2.6 µM) and PO_4^{3-} (0.3–2.9 µM) were generally lower in surface than in bottom waters (Table S1). Reflecting the known eutrophication gradient in WLIS, water clarity increased from west to east (1.2–2.0 m), while chl *a* concentration and microzooplankton biomass generally decreased towards the east (Fig. 2D,E). Chl *a* had similar concentrations in July and August, but higher values in surface (6.6–18.8 µg l^{-1}) than bottom waters (1.2–4.7 µg l^{-1}). Microzooplankton biomass was also higher in surface (10.7–122.6 µg C l^{-1}) than bottom waters (0.4–2.5 µg C l^{-1}, except for the westmost value of 20.3 µg C l^{-1} during both sampling periods), but reached values 1 order of magnitude higher in August than in July (Fig. 2E). Dinoflagellates dominated microzooplankton biomass, except for the prevalence of ciliates in the westmost station during July and 1 bottom sample in August, and nauplii in the remaining August bottom samples (Fig. 2F).

3.2. Taxonomic diversity of bacteria, archaea and microeukaryotes

We obtained 1920 and 1314 final ASVs based on 16S and 18S, respectively. Considering both datasets,

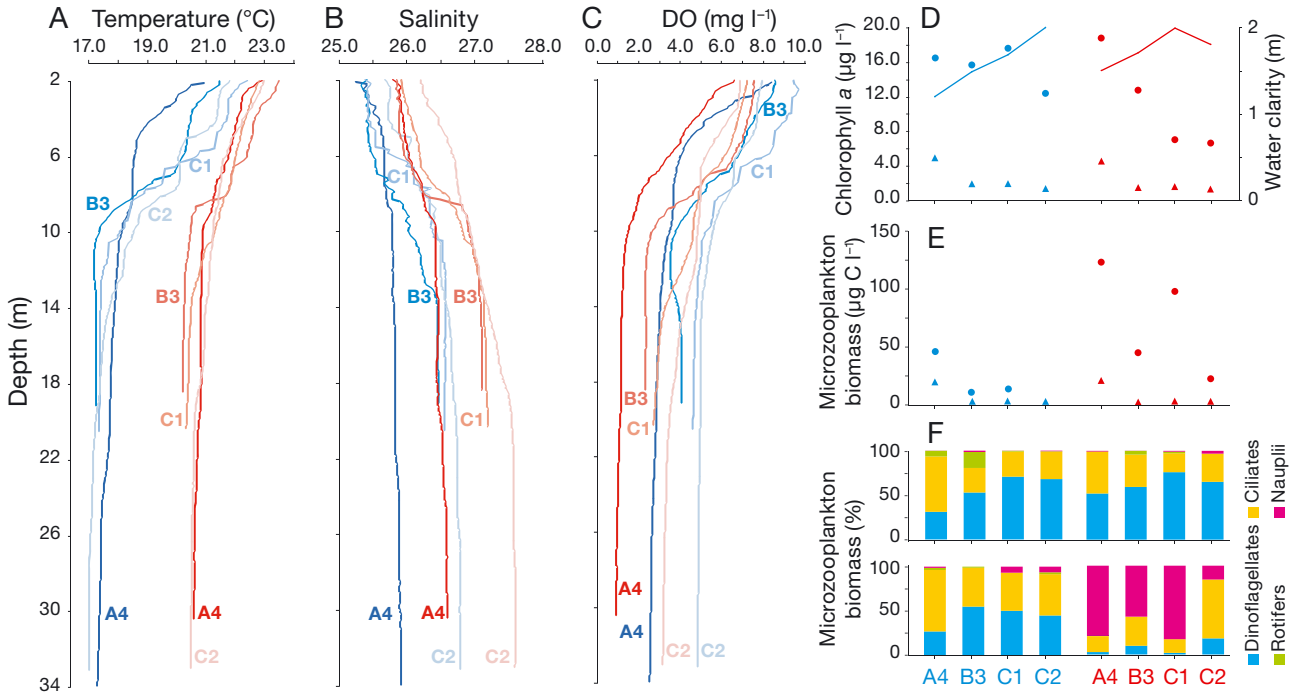

Fig. 2. General abiotic and biotic conditions in July (red palette) and August (blue palette) at Stns A4, B3, C1 and C2. (A–C) Vertical profiles showing the thermohaline stratification of the water column and the decrease of dissolved oxygen (DO) in bottom waters. (D,E) West-to-east gradient of eutrophication as indicated by water clarity (line) and surface (circle) and bottom (triangle) plankton estimates. (F) Microzooplankton proportions in surface (upper panel) and bottom (lower panel) waters. (A–D) Data from the Connecticut Department of Energy and Environmental Protection

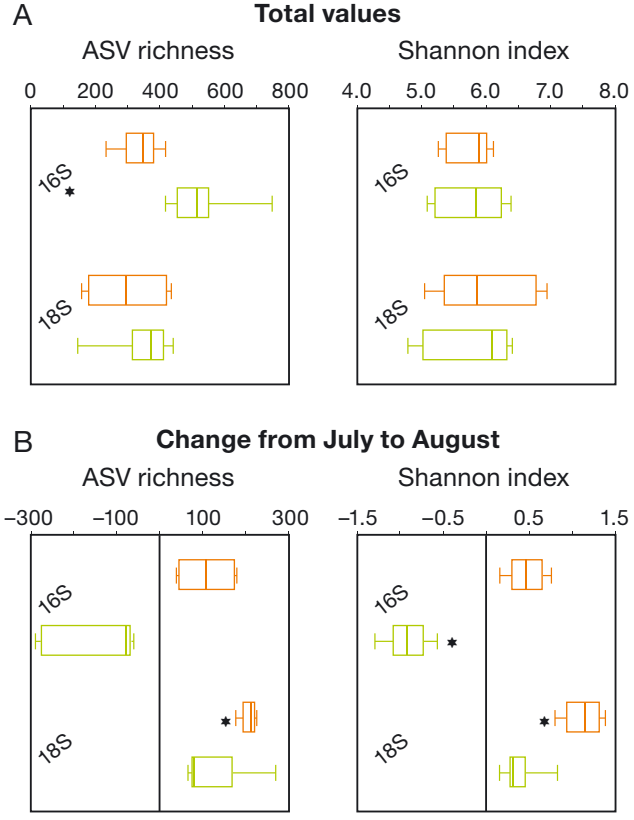

Fig. 3. Alpha-diversity based on 16S and 18S sequences in surface (orange) and bottom (green) waters. (A) Total values for each marker and depth (July and August values are pooled). (B) Change from July to August. ASV: amplicon sequence variants. Each boxplot shows the median (thick line), interquartile (box) and range (whiskers). *Significant differences (pairwise *t*-test; $p < 0.01$): (A) between surface and bottom waters or (B) from July to August

alpha-diversity overlapped in ranges of observed ASV richness (141–747) and Shannon index (4.7–6.9) (Fig. 3A). The only significant difference between sampling depths corresponded to 16S ASV richness, which was higher in bottom than surface waters. Alpha-diversity also presented some significant changes from July to August (Fig. 3B). In surface waters, alpha-diversity increased from July to August, although this change was only significant for 18S. In bottom waters, 18S-based alpha-diversity also increased, but not significantly. On the other hand, 16S-based alpha-diversity decreased from July to August in bottom waters, and this change was significant in terms of the Shannon index.

The 16S dataset was dominated by the bacterial phyla *Proteobacteria* (mainly *Alphaproteobacteria*,

39%, and *Gammaproteobacteria*, 22%), *Bacteroidetes* (11%) and *Actinobacteria* (8%), and the archaeal phylum *Thaumarchaeota* (7%) (Fig. 4A, Table S2). The taxonomic composition differed under maximum hypoxia (August, bottom) versus the rest of the samples, with a decreased proportion of most bacterial phyla (25%) and an increase in *Thaumarchaeota* (21%) and *Nitrospinae* (2%) under maximum hypoxia. Other changes in relative abundance were not associated with time but rather with sampling depth, specifically a 6% decrease of *Cyanobacteria* in bottom versus surface waters during both sampling periods.

The 18S dataset was dominated by Dinophyceae dinoflagellates (38%) and Diatomea (16%), followed by Syndiniales dinoflagellates (10%) and Copepoda (9%) (Fig. 4B, Table S2). The taxonomic composition differed under maximum hypoxia versus the rest of the samples mainly by an increase in Copepoda (26%), Kathablepharidacea (2%) and Bigyra (3%). Other changes in relative abundance were linked to sampling depth, specifically decreases in Diatomea (17%) and Chlorophyta (6%) and an increase in Syndiniales (10%) in bottom versus surface waters during both sampling periods.

Beta-diversity analyses supported differences in both prokaryotic and eukaryotic communities across samples (Fig. 4C,D). ANOSIM indicated significant differences for samples collected during maximum hypoxia (August, bottom) versus the rest of the samples (16S: R = 0.67, p = 0.005; 18S: R = 0.56, p = 0.001). The communities also differed significantly for samples grouped by date and depth (16S: R = 0.88, p = 0.001; 18S: R = 0.99, p = 0.001).

3.3. Distribution of dominant ASVs

Among the ASVs that dominated the 16S data (Fig. 5A), some had high relative abundances (>5%, maximum: 22%) in all or most samples (e.g. 2 ASVs assigned to the *Alphaproteobacteria*, SAR11 clade Ia), while others showed decreased proportions under maximum hypoxia (e.g. 2 ASVs affiliated to *Alphaproteobacteria* SAR116 and *Gammaproteobacteria* SAR86 with proportions up to 5% in non-hypoxia, but lower than 1% in most hypoxic samples). Instead, the dominant ASV under maximum hypoxia (which peaked at a 29% contribution and corresponded to the *Thaumarchaeota* genus *Nitro-*

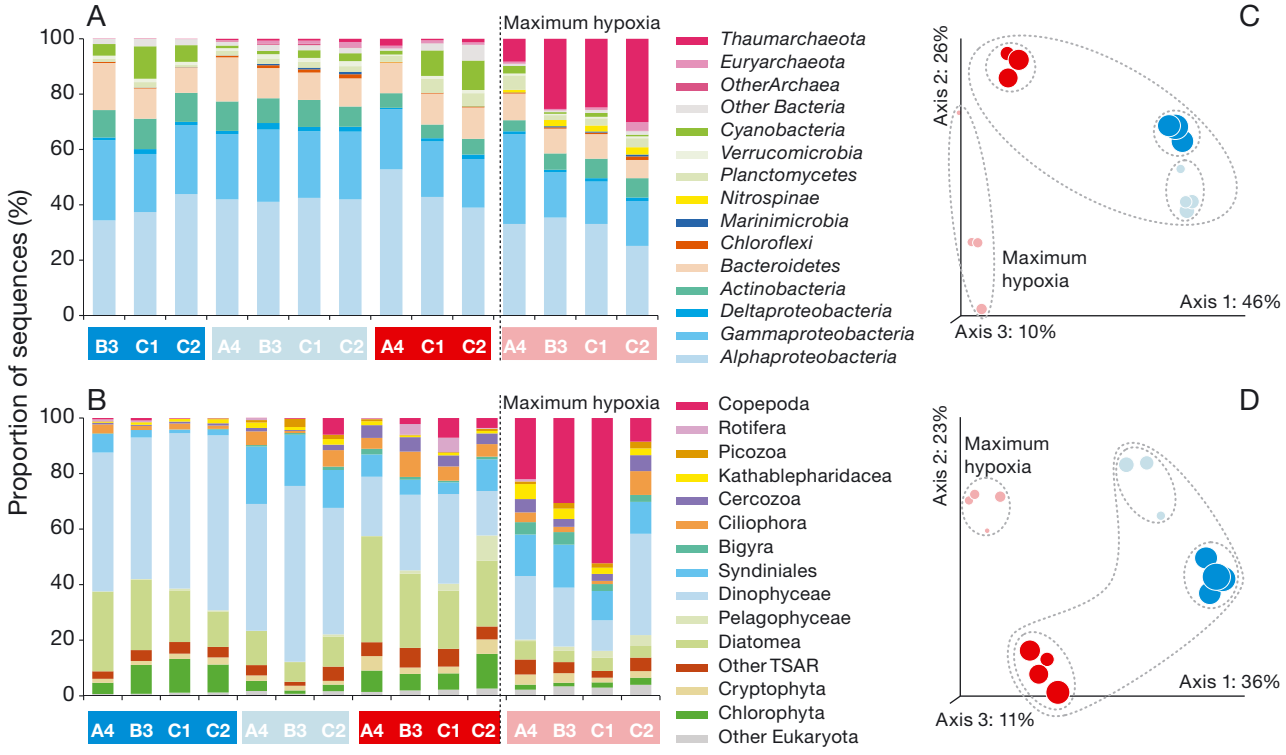

Fig. 4. Community structure based on (A,C) 16S and (B,D) 18S sequences from samples collected in July (blue palette) and August (red palette) in surface (darker) and bottom (clearer) waters. (A,B) Relative abundances of major taxonomic groups (see also Table S2). (C,D) Principal coordinates analyses based on Bray-Curtis dissimilarity among samples. The percentages of variance explained by each axis are shown. Samples are indicated by bubbles size-scaled based on dissolved oxygen (0.9–9.4 mg l^{-1}). Dotted shapes indicate sample groups that showed significant differences based on ANOSIM (see Section 3.2)

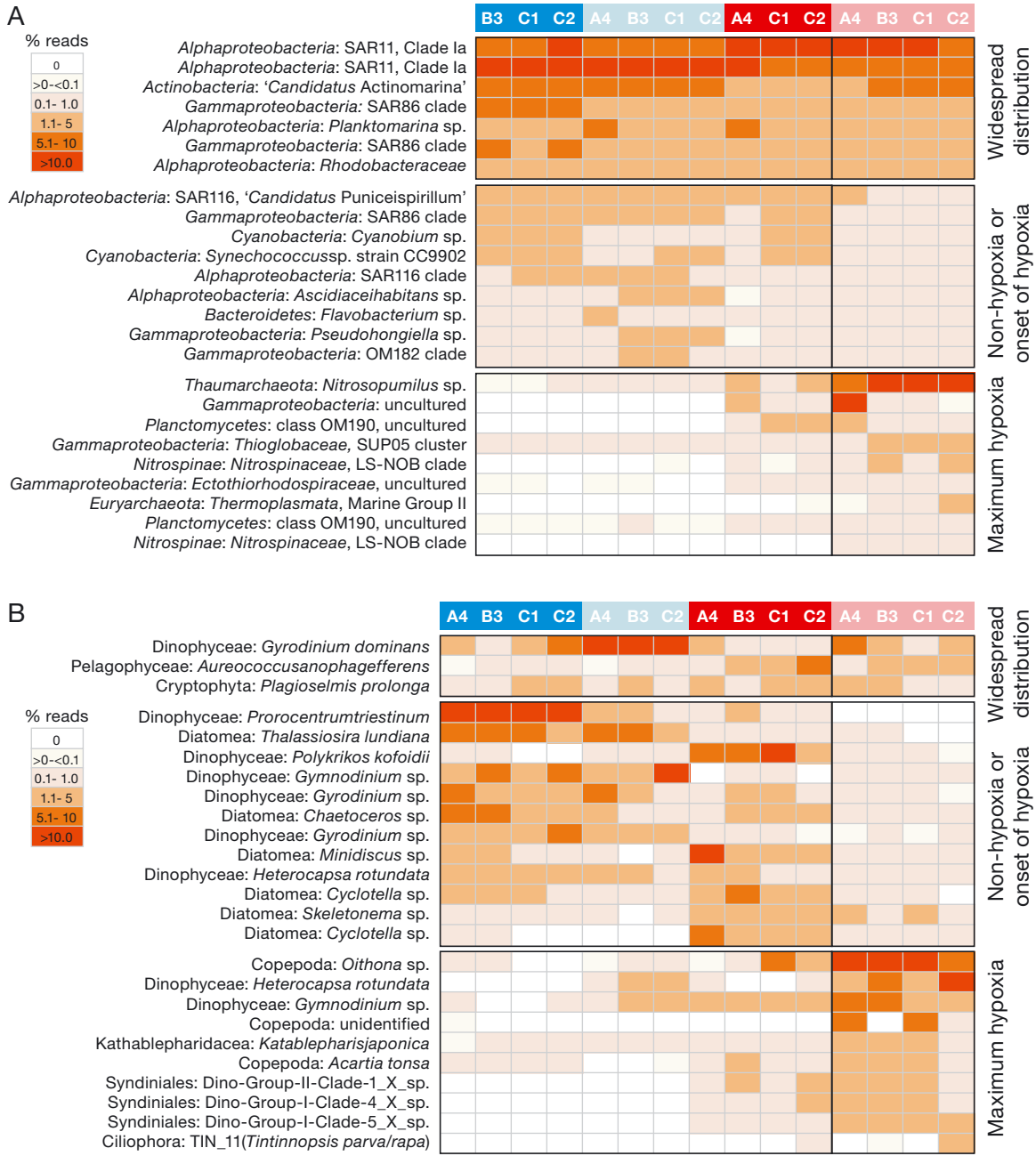

Fig. 5. Distribution of the dominant (A) 16S and (B) 18S amplicon sequence variants (ASVs) in samples collected in July (blue palette) and August (red palette) in surface (darker) and bottom (clearer) waters. Heatmaps (orange palette) based on relative abundances out of total reads per sample. The shown ASVs represent 65% and 50% of the total 16S and 18S reads, respectively, and are partitioned based on their prevalence under maximum hypoxia, the rest of the samples or everywhere

sopumilus) was much less prevalent in the rest of the samples. Other ASVs were detected exclusively under maximum hypoxia (e.g. within the *Nitrospinae*, *Nitrospinaceae* LS-NOB clade and the *Euryarchaeota*, *Thermoplasmata* Marine Group II).

Among the ASVs that dominated the 18S data (Fig. 5B), only 3 (identified as the dinoflagellate *Gyrodinium dominans*, the pelagophyte *Aureococcus anophagefferens* and the cryptophyte *Plagioselmis prolonga*) were homogeneously distributed across samples. The most prevalent ASVs under maximum hypoxia were found in much lower proportions or were not detected in the rest of the samples, and vice versa. For example, one ASV identified as the

copepod *Oithona* sp. represented up 41% of the reads in August bottom waters, but contributed 0–6% in the rest of the samples. In contrast, one ASV identified as the dinoflagellate *Prorocentrum triestinum* was not detected under hypoxia but was present in all other samples, with a proportion up to 26%.

There were ASVs restricted by sampling date rather than oxygenation level (Fig. 5). For example, there were ASVs only detected in August based on either 16S (e.g. one ASV identified as an uncultured *Gammaproteobacteria* and another one affiliated to *Planctomycetes*, class OM190) or 18S (3 ASVs classified in the Syndiniales, Dino-Group-I or Dino-Group-II).

3.4. Predictions of functional diversity of bacteria and archaea

Functional potential based on the 16S dataset (PICRUSt2 analysis) included mostly matches to housekeeping pathways, such as metabolism of carbohydrates, amino acids, fatty acids and nucleotides (Table S3). The samples collected during maximum hypoxia (August, bottom) displayed a higher heterogeneity in MPs compared to the rest of the samples (Fig. 6A), and ANOSIM indicated significant differences between both sample groups ($R = 0.95$, $p = 0.001$).

Compared to the rest of the samples, the MPs most overrepresented under maximum hypoxia included anaerobic or archaea-specific processes, such as synthesis of cofactors (e.g. coenzyme F420, a redox-active compound in archaeal methanogenesis), a reductive acetyl CoA pathway (a type of CO_2 fixation in the strictly anaerobic homoacetogenic bacteria) and nitrifier denitrification (Fig. 6B). The MPs most underrepresented under maximum hypoxia included mainly aerobic bacterial processes for fatty acid biosynthesis, degradation of carbohydrates and aromatic compounds, and oxidation of C1-compounds (a CO_2-producing process in methylotrophic bacteria).

3.5. Correlations between community structure and environmental factors

Alpha-diversity values based on 16S or 18S ASV richness or Shannon index were generally not correlated to the environmental variables we measured (not shown). Only 16S ASV richness showed significant and inverse relationships with temperature ($R = -0.80$, $p < 0.01$), chl *a* concentration ($R = -0.68$, $p < 0.01$) and, less significantly, with DO ($R = -0.56$, $p < 0.05$).

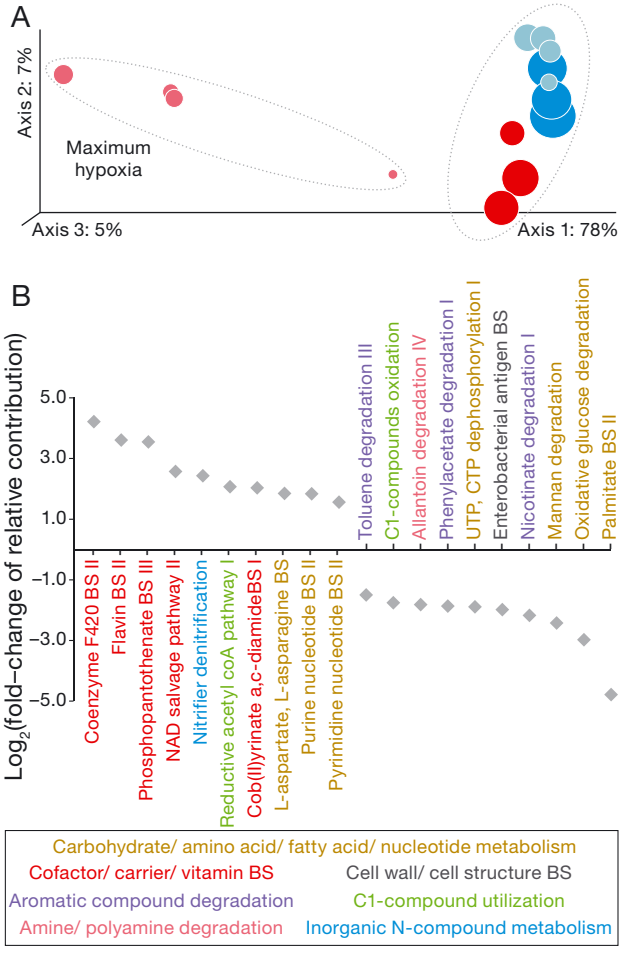

Fig. 6. Predicted functional diversity of bacteria and archaea. (A) Principal coordinates analysis of 16S-derived metabolic pathways (MPs); explanations as in Fig. 4C. (B) Top 10 MPs over- and underrepresented under maximum hypoxia as compared to the rest of the samples. BS: biosynthesis. Pathways according to https://metacyc.org/

Beta-diversity matrices based on 16S, 16S-based MPs or 18S datasets (Figs. 4C,D & 6A) were significantly correlated ($p < 0.05$) with the environmental variables we measured (Mantel test; Table 1). The combination of temperature, salinity and/or DO best explained the distributions of prokaryote and eukaryote communities across all samples (BIO-ENV; Table 1). When the analyses were restricted to samples with available nutrient data, then nutrient concentrations (most frequently NO_x^-) were best correlated with community structure (BIO-ENV; Table 1).

Table 1. Relationship between community structure and environmental variables. Comparisons based on 16S and 18S amplicon sequence variants and 16S-based metabolic pathways (MPs)

Dataset	Mantel test R	Mantel test p	BIO-ENV test Top 2 subsets of variables that best correlate with beta-diversity
16S[a]	0.49	0.003	Temperature + Salinity
			Temperature + Salinity + Dissolved oxygen
16S[b]	0.35	0.063	Temperature + Nitrate plus nitrite + Orthophosphate
			Nitrate plus nitrite + Orthophosphate
MPs[a]	0.31	0.022	Salinity
			Salinity + Dissolved oxygen
MPs[b]	0.32	0.180	Nitrate plus nitrite
			Nitrate plus nitrite + Orthophosphate
18S[a]	0.50	0.002	Temperature + Salinity + Dissolved oxygen
			Temperature + Salinity + Dissolved oxygen + Chlorophyll *a*
18S[b]	0.68	0.003	Temperature + Salinity + Nitrate plus nitrite + Ammonium + Orthophosphate
			Salinity + Nitrate plus nitrite + Ammonium + Orthophosphate

Datasets include: [a]all samples or [b]only samples with available nutrient data (see Table S1). R = Pearson's coefficient

4. DISCUSSION

Our results show that the conditions associated with the intensification of hypoxia in the bottom waters of WLIS during summer 2019 correlated with significant changes in the diversity, community structure and potential functioning of microbial communities (Figs. 3–6, Table 1). Because of increased temperatures, seasonal stratification, and eutrophication, this area experiences hypoxia every summer. Although the hypoxic episode was weaker in 2019 compared to previous years, it was sufficient to cause quantifiable changes in the taxonomic structure of the microbial food web and to potentially influence nutrient recycling in the water column. Our results suggest that the detected impacts on bacteria, archaea and microeukaryotes were likely not due to deoxygenation per se, but rather a consequence of the overall conditions resulting from the interaction of physical, chemical and biological factors in the area as summer progressed (Table 1). One constraint of this study is that the limited number of discrete samples does not capture fine-scale spatial and temporal variations in oxygenation levels. Still, we detected significant shifts in microbial communities that are consistent with our hypothesized increases in the proportions of archaea and bacterivore protists and changes in the potential for oxygen-sensitive metabolisms during hypoxia.

4.1. Changes in prokaryotic diversity and community structure

The diversity and taxonomic composition of bacteria and archaea changed significantly between non-hypoxic and hypoxic conditions. ASV richness was significantly lower in the well-oxygenated surface waters than in the bottom during the 2 periods investigated (Fig. 3A), and thus overall ASV richness was inversely correlated with DO ($R = -0.56$, $p < 0.05$). An increase in prokaryotic diversity as DO levels decrease agrees with findings in other hypoxic estuaries, such as the Hood Canal in the Northwest USA (Spietz et al. 2015) and the Changjiang estuary in China (Wu et al. 2019), or across an oceanic OMZ (eastern tropical North Pacific Ocean; Beman & Carolan 2013), and it may be explained by habitat heterogeneity across the oxycline, where contiguous niches overlap. In WLIS bottom waters, however, intensification of hypoxia as summer progressed was associated with a decrease in prokaryotic alpha-diversity (Fig. 3B).

The prokaryotic community structure was dominated by typically marine and estuarine lineages. The fact that the dominant ASVs were relatively abundant in all our samples (Fig. 5A) reflects the tolerance to changes in oxygenation in these lineages, including ASVs within the *Alphaproteobacteria* SAR11 clade Ia, *Rhodobacteraceae* (including *Planktomarina*) and the *Gammaproteobacteria* SAR86. These lineages are ubiquitous in normoxic estuarine and marine waters and are also common under hypoxia (Crump et al. 2007, Wright et al. 2012, Spietz et al. 2015). This uniform distribution of dominant ASVs contrasts with the partitioning of sequences among phyla, which was quite homogeneous in non-hypoxia but distinct under maximum hypoxia (Fig. 4A). Thus, except under maximum hypoxia, the significant differences among sample groups by date and depth (Fig. 4C) were mostly due to replacement of non-dominant ASVs within the same phyla. Another exception corresponds to *Cyanobacteria* (represented mostly by the ubiquitous *Synechococcales* genera *Cyanobium* and *Synechococcus*), which did not show an influence of hypoxia, but instead of depth, as ex-

pected, given the influence of light availability on photosynthesis (Fig. 4A). Overall, while date- and depth-specific factors likely influenced distribution patterns, the main change in community structure was between maximum hypoxia and the rest of the samples (Fig. 4C).

The main change in 16S-based community composition as hypoxia intensified was an increase in archaeal proportions (Fig. 4A). While the proportions of several of the most abundant ASVs (all bacterial) decreased sharply, the most conspicuous increase in relative abundance under maximum hypoxia corresponded to a single ASV classified within the *Thaumarchaeota* genus *Nitrosopumilus* (Fig. 5A). This ASV has a 100% BLAST match (E-value < 10^{-100}) to >1000 sequences in NCBI GenBank, including strains of *N. maritimus* isolated from a tropical marine fish tank (Walker et al. 2010), Puget Sound in the Northwest USA (Qin et al. 2017) and the Pacific Ocean (Ahlgren et al. 2017), as well as environmental sequences from hypoxic waters of the Gulf of Mexico (Tolar et al. 2013). *Nitrosopumilus* is among the dominant archaeal genera in hypoxic waters (e.g. Smith et al. 2013, Parsons et al. 2015, Zou et al. 2020) and the main ammonia-oxidizers in marine and estuarine environments (Damashek & Francis 2018, Santoro et al. 2019).

Bacteria that we detected almost exclusively under maximum hypoxia are characteristic of low oxygen conditions (Fig. 5A). The *Planctomycetes* class OM190 has been reported in hypoxic sediment (Ye et al. 2016). The *Thioglobaceae* SUP05 cluster (*Gammaproteobacteria*) is the most abundant bacterial group in suboxic and anoxic waters according to a meta-analysis of diverse OMZs (Wright et al. 2012). The *Nitrospinaceae* uncultured LS-NOB clade (*Nitrospinae*) is related to the genus *Nitrospina*, which we also detected exclusively under hypoxia, but in low proportions. This genus is among the most common nitrite-oxidizing bacteria (NOB) in hypoxic waters of estuaries (Spietz et al. 2015, Hou et al. 2018) and OMZs (Wright et al. 2012, Lücker et al. 2013, Sun et al. 2019).

In agreement with the shift in taxonomic composition under maximum hypoxia, there was a clear, significant differentiation in potential functional diversity versus the rest of the samples (Fig. 6A). On the PCoA, samples under maximum hypoxia are much more spread out on the axis 1 compared to all the other samples, thus reflecting a wider variety of MPs (Fig. 6A). In low-oxygen waters, aerobic and anaerobic microbial processes co-occur as a consequence of gradients in oxygen sensitivity and biochemical adaptations to energy substrates (Bertagnolli & Stewart 2018). Even though we did not detect anoxia in WLIS, DO was low enough to favor taxa that potentially have genes for 2 anaerobic reductive pathways, methanogenesis and homoacetogenesis (Fig. 6B), possibly associated to particles resuspended from anoxic sediment or forming anoxic microniches (Smith et al. 2013). We also detected potential changes in N-cycling pathways during maximum hypoxia (see Section 4.3). Functional predictions based on 16S sequences are limited by the power of this gene to resolve ecologically different units and by the relatively low availability of reference genomes from environmental prokaryotes (Douglas et al. 2020). Still, this approach can provide preliminary insights on potential metabolic and biogeochemical differences under distinct environmental conditions (e.g. Ward et al. 2017, Quero et al. 2020), as observed here in hypoxia versus normoxia. With a different set of limitations, metatranscriptomic profiles of microbial plankton in Chesapeake Bay confirmed a switch from aerobic to anaerobic metabolism along with summer deoxygenation of bottom waters, although differences were better explained by depth than DO (Hewson et al. 2014).

4.2. Changes in microeukaryotic community structure

Microeukaryotic alpha-diversity did not change significantly as hypoxia intensified in bottom waters, contrary to the decrease we observed for prokaryotes (Fig. 3) or that is usually observed for fish and benthic animals (Vaquer-Sunyer & Duarte 2008). For protists, strong reductions in abundance and diversity (richness and evenness) were reported after an episodic but more extreme hypoxia event in a semi-enclosed human-made harbor in the Southwest USA coast (Stauffer et al. 2013). It is possible that the hypoxic conditions in WLIS were not strong enough to significantly change protist diversity.

Like prokaryotes, the microeukaryotic community consisted predominantly of typical estuarine and marine lineages, but only 3 ASVs were both dominant and widespread in all samples (Fig. 5B). These included the microzooplankton *Gyrodinium dominans*, the picoplankton alga *Aureococcus anophagefferens* (which is known to form harmful algal blooms in Long Island embayments; Gobler et al. 2011), and the nanoplankton alga *Plagioselmis prolonga* (which was recently proven to be a life stage of *Teleaulax amphioxeia*, the chloroplast source for the mixotrophic, red tide ciliate *Mesodinium rubrum*;

Altenburger et al. 2020). The ASVs that dominated under hypoxia or in the rest of the samples showed more limited distributions, thus suggesting a lower metabolic flexibility compared to prokaryotes (see Section 4.1). The significant differences in beta-diversity between maximum hypoxia and the rest of the samples (Fig. 5D) are both due to changes in ASV distribution (Fig. 5B) and composition of major taxa (Fig. 4B), although sampling date and depth had a stronger influence than for prokaryotes.

Under non-hypoxia, sequences corresponding to phytoplankton and grazers prevailed. A higher prevalence of diatoms and chlorophytes in surface than in bottom waters is not surprising due to light availability for photosynthesis (Fig. 4B, Table S2); this is also consistent with higher chl *a* levels in the surface (Fig. 2D). The constitutive mixotroph *Prorocentrum triestinum* also prevailed in surface waters, especially in July (Fig. 5B), consistent with observations of *Prorocentrum* blooms during this period (D. I. Greenfield unpubl. data). While not evident during our survey, this species can form red tides that lead to hypoxia in eutrophic coastal waters (Ndhlovu et al. 2017). The prevailing grazers in surface waters and also in July bottom waters were dinoflagellates, especially *Gyrodinium* spp. and *Polykrikos kofoidii*. Their grazing pressure, however, was likely insufficient to consume the summer primary production, given that hypoxia intensified in August as expected due to phytoplankton decomposition.

Elucidating the functional diversity of eukaryotic microbial communities presents many challenges (reviewed by Santoferrara et al. 2020) and lags behind compared to prokaryotes. Still, we observed changes in eukaryotic sequence proportions that suggest a switch from autotrophy to heterotrophy dominance under maximum hypoxia. The main shift in community structure was a decreased contribution in diatoms and primarily autotrophic dinoflagellates (except for the known or potential constitutive mixotrophs *Heterocapsa rotundata* and *Gymnodinium* sp., respectively). Instead, there was an increase in the relative abundance of heterotrophic nano- and picoflagellates (e.g. *Katablepharis japonica*) and copepods (e.g. *Oithona* sp., *Acartia tonsa*) (Figs. 4B & 5B, Table S2). The increased proportions of heterotrophic nano- and picoflagellates, including the Bigyra MAST-6 and MAST-12, suggests increased bacterivory (Massana et al. 2014), as expected, given the potentially increased prokaryotic abundances associated with decomposition activity during hypoxia. On the other hand, we did not detect bacterivorous ciliates typical of hypoxic conditions (e.g. *Uronema*; Dolan & Coats 1991, Stauffer et al. 2013) or any known anaerobic ciliate (Fenchel & Finlay 1991).

While the increased proportions of copepod sequences in August may follow a seasonal signal, maximum contributions in bottom waters (Figs. 4B & 5B) were unexpected, given that these microcrustaceans are generally less abundant under hypoxia (Keister et al. 2000, Roman et al. 2012, Elliott et al. 2013). Because of known biases in relative abundances based on 18S rRNA gene sequences (e.g. due to multicellularity and multiple copies of rRNA genes per cell; Santoferrara 2019), we corroborated by microscopy that copepod biomass increased from non-hypoxic to hypoxic conditions, both in relative (Fig. 2F) and absolute values (from 0.3 to 4.9 µg C l^{-1} on average). Neither of the 2 methods, however, allow us to determine if the detected copepods (nauplii and other stages smaller than 200–450 µm) were alive at the time of sampling. Studies using a vital stain have concluded that most *A. tonsa* nauplii under hypoxic conditions in Chesapeake Bay are dead, possibly trapped after egg hatching in bottom waters (Elliott et al. 2013). Others, instead, have proposed that taxon-specific differences and regional adaptations may allow some estuarine copepod species to use hypoxic waters as a refuge from predators (Auel & Verheye 2007, Ludsin et al. 2009). Species within *Oithona* are even proposed as indicators of eutrophication and hypoxia, given that they can proliferate in estuaries under degraded conditions (e.g. in Puget Sound; Keister & Tuttle 2013). Either alive or dead, the increased proportion of copepods can have important consequences on carbon export and N cycling under hypoxia (see Section 4.3).

Syndiniales had higher proportions in bottom waters (Fig. 4B), and some ASVs detected only in August were among the dominant ones under maximum hypoxia (Fig. 5B). Syndiniales are parasitic dinoflagellates that infect a wide range of planktonic hosts, from other dinoflagellates and ciliates to copepods and other zooplankton, which results in their frequent dominance of environmental DNA sequences (Skovgaard 2014). For example, Syndiniales Groups I and II were among the prevailing protists in a seasonally deoxygenated fjord of the Northwest Canada coast (Saanich Inlet), with the highest relative abundances in suboxic and anoxic waters (Torres-Beltrán et al. 2018). Based on rDNA:rRNA ratios, the same study suggested that some Syndiniales OTUs corresponded to inactive sinking cells, while others were from cells actively parasitizing or being ingested by other organisms in deep waters. The Syndiniales ASVs that dominated in WLIS under

hypoxia also correspond to Groups I and II, and 2 are closely related to *Amoebophrya* and *Euduboscquella* (Group II clade 1 and Group I clade 4, respectively). Species in *Amoebophrya* and *Euduboscquella* can cause mortality rates high enough to control phytoplankton blooms (including harmful algal blooms; Chambouvet et al. 2008) and microzooplankton populations (Coats & Heisler 1989), respectively, in estuarine waters. Thus, one possibility is that parasitism contributes to organic carbon release by cell lysis and plays an important role in the planktonic food web, possibly exceeding mortality by zooplankton grazing if/when they are impaired by hypoxia.

4.3. Potential changes in the N cycle

Pollution with N compounds and their subsequent reactions define the trajectory of eutrophication and hypoxia in estuaries. The N cycle is a complex network of processes that are driven by bacteria and archaea that oxidize or reduce N species in their energy metabolism (Ward 2013, Kuypers et al. 2018) and is influenced by feedbacks with plankton and DO. In brief, excess NH_4^+ and NO_3^- (the dominant forms of reactive N in estuaries) are assimilated as phytoplankton biomass, with the resulting organic N eventually being remineralized into NH_4^+ and then sequentially oxidized to NO_2^- and NO_3^- by nitrification at the expense of DO; if DO is low enough in the bottom waters or underling sediments, NO_x^- are reduced by either denitrification to N gases lost to the atmosphere (N_2O, N_2) or dissimilatory nitrate reduction to NH_4^+ that is effectively recycled in the estuary (Damashek & Francis 2018). Disentangling these processes requires rate measurements not done in the present study, but discrete data on N nutrients and microbial communities can provide snapshots of potential N metabolism in the water. Complementing our nutrient data with monthly estimates by CT DEEP shows that the concentrations of NH_4^+ and NO_x^- were relatively stable in WLIS during summer 2019, except for the maximum NO_x^- value we detected in August bottom waters (Fig. A1 in the Appendix). Because our data showed concurrent increases in the concentration of NO_x^- and the proportion of N-cycling prokaryotes during maximum hypoxia (Table S1, Figs. 4A, 5A & 6B), we looked specifically at predicted N-cycling pathways in our PICRUSt2 annotation of 16S sequences (Fig. 7). Given the limitations of this approach (see last paragraph of Section 4.1), our preliminary results need confirmation with direct quantification of N-cycling genes and their expression. Still, these data allow us to explore potential N transformations that can be important in estuarine waters but have been studied much less than in sediments (Damashek & Francis 2018), and to generate hypotheses to be tested with more appropriate tools (e.g. qPCR) at a higher spatial-temporal resolution.

The main difference in functional potential between hypoxic and non-hypoxic conditions in our study did not correspond to classical N pathways according to PICRUSt2 (Fig. 7). Instead, the potential for nitrifier denitrification was over-represented under maximum hypoxia (Figs. 6B & 7). In this path-

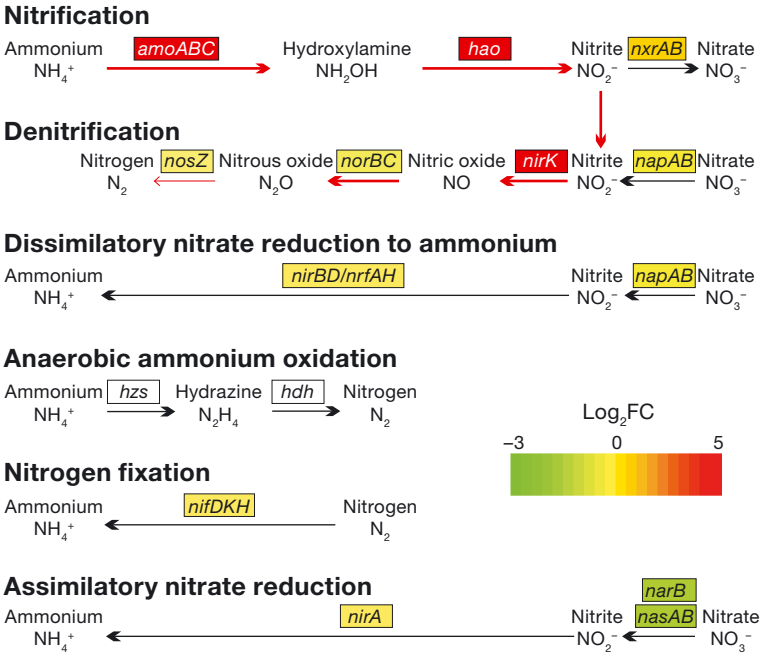

Fig. 7. Predicted bacterial and archaeal genes for metabolism of inorganic nitrogen compounds based on PICRUSt2 annotations. Genes are colored based on predicted over- and underrepresentation in maximum hypoxia as compared to the rest of the samples; FC: fold-change of the relative contribution of KEGG orthologs (KOs) in each sample group. Red arrows: the nitrifier denitrification pathway. Genes in white are not predictable by this method, but taxa known to have them were not found in our data. Predicted genes: *amoABC*: ammonia monooxygenase; *hao*: hydroxylamine dehydrogenase; *nxrAB*: nitrite oxidoreductase; *napAB*: nitrate reductase; *nirK*: nitrite reductase (NO-forming); *norBC*: nitric oxide reductase; *nosZ*: nitrous-oxide reductase; *nirBD*: nitrite reductase (NADH-forming); *nrfAH*: nitrite reductase (cytochrome *c*-552); *hzs*: hydrazine synthase; *hdh*: hydrazine dehydrogenase; *nifDKH*: nitrogenase; *narB*: ferredoxin-nitrate reductase; *nasAB*: assimilatory nitrate reductase; *nirA*: ferredoxin-nitrite reductase

way, ammonia (available in the water mostly as NH_4^+) is oxidized to NO_2^-, which is then reduced to nitric oxide (NO) and nitrous oxide (N_2O) and, only partially, to N_2 (Ritchie & Nicholas 1972, Wrage-Mönnig et al. 2018). Although nitrifier denitrification is technically classified as anaerobic respiration, it is speculated to function in the detoxification of NO_2^- produced by nitrification rather than in anaerobic energy production (Stein & Arp 1998, Beaumont et al. 2002), and it is more active in hypoxia than anoxia (Zhu et al. 2013, Kozlowski et al. 2014). Of the taxa known to perform nitrifier denitrification, we only found the ammonia-oxidizing bacteria (AOB) *Nitrosomonas* (*Gammaproteobacteria*), which we detected almost exclusively under maximum hypoxia but in negligible proportions (<0.02%; not shown). However, the genome of the ammonia-oxidizing archaea (AOA) *Nitrosopumilus maritimus*, which had increased proportions under maximum hypoxia (Figs. 4A & 5A), includes genes that may participate in this pathway (*amoABC*, hypothetical *hao* and *nirK*; Walker et al. 2010). This explains the over-representation of these genes under maximum hypoxia in our annotations (Fig. 7) and suggests potentially increased ammonia oxidation coupled with NO_2^- reduction to NO under these conditions. We did not detect a simultaneous increase in potential for biotic reduction of NO to N_2O (Fig. 7), but this reaction can happen abiotically in marine waters (Zhu-Barker et al. 2015). While the mechanisms are not fully understood, AOA (mainly the order *Nitrosopumilales*) are the main contributors to AO-associated N_2O production in coastal and oceanic waters (Santoro et al. 2011, 2019, Löscher et al. 2012, Trimmer et al. 2016), and their activity is important in the global production of this powerful greenhouse gas (Prosser et al. 2020).

Alternatively, ammonia oxidation by *Nitrosopumilus* AOA may be coupled with oxidation of NO_2^- to NO_3^-, which completes the classical nitrification pathway. However, our data supported only a moderate increase in potential for this reaction (*nxrAB* genes; Fig. 7) by the *Nitrospinaceae* NOB detected under hypoxia (Figs. 4A & 5A). Decoupling of NH_4^+ and NO_2^- oxidation has been found experimentally at temperatures between 20 and 30°C in estuarine waters, resulting in NO_2^- accumulation during summer (Schaefer & Hollibaugh 2017). Thus, the summer peak of NO_x^- in bottom waters that we detected in August (maximum: 14.4 µM; Table S1), in agreement with much higher proportions of AOA than NOB (Figs. 4A & 5A), may have been in the form of NO_2^- and not as the expected NO_3^-.

Canonical denitrification, dissimilatory nitrate reduction to ammonium (DNRA), and anaerobic ammonium oxidation (anammox) were not supported by our data, as expected under non-anoxic conditions, even though low expression levels for denitrification and DNRA genes have been detected in hypoxic waters of Chesapeake Bay (Hewson et al. 2014, Eggleston et al. 2015). Coincidently, we detected potential for denitrification and DNRA, but it was quantitatively small (not shown) and it did not change with oxygenation level (Fig. 7). The later also applies to N_2 fixation and assimilatory nitrate reduction, although the potential for reduction of NO_3^- to NO_2^- (*narB* and *nasAB* genes) was higher in non-hypoxic versus hypoxic conditions (Fig. 7), at least partially matching the distribution of *Cyanobacteria* (Fig. 4A).

Our data also provide insights on the coupling between biogeochemical and food web processes and its feedback with hypoxia. The increased proportions of AOA (*Nitrosopumilus*) and NOB (*Nitrospinaceae*) could be related to multiple factors, such as differential grazing that may favor these lineages at low DO levels or intensified dynamics of N species during the summer. Increases in the relative abundance of *Nitrosopumilus* and *Nitrospinaceae* co-occurred with increased proportions of copepod nauplii and increased concentration of NO_x^- in August bottom waters (Figs. 2F, 4 & 5, Table S1). This suggests that N passed through phytoplankton and then copepods before remineralization to NH_4^+ and subsequent oxidation to NO_x^-. Copepods stimulate nitrification mainly via excretion of NH_4^+ and dissolved organic N (Valdés et al. 2018), or via decomposition if they are dead. Thus, *Nitrosopumilus* and *Nitrospinaceae* could have been stimulated by copepods, as suggested by the sequence proportions of the 2 genera being positively and significantly correlated with the proportion of copepod sequences and biomass we estimated ($R > 0.66$, $p < 0.01$). The proportions of *Nitrosopumilus*, *Nitrospinaceae* and Copepoda sequences also correlated positively and significantly with the concentration of NO_x^- ($R > 0.98$, $p < 0.01$), but not NH_4^+. This suggests that, although hypoxia was at its summer maximum, DO was enough for remineralization of organic N and rapid oxidation of NH_4^+, thus resulting in the observed accumulation of NO_x^- in August bottom waters (Table S1, Fig. A1 in the Appendix). These preliminary results agree with the expectation of active recycling of C and N in WLIS in the summer, with excess primary production stimulating grazers, which in turn stimulate the bacterial and archaeal N-oxidizing metabolisms that contribute to hypoxia.

5. CONCLUSIONS

As oxygen-limited aquatic regions rapidly expand around the world, knowledge on the microbial communities that interact with decreased DO is important to predict future scenarios under global anthropogenic changes. Among the various types of environments experiencing deoxygenation, we studied a temperate estuary that undergoes summer hypoxia due to cultural eutrophication. Our results complement existing knowledge by providing a holistic view of the microbial communities (bacteria, archaea and microbial eukaryotes) that form the base of the food web and drive important biogeochemical cycles. In surface waters, N pollution fuels phytoplankton, which in turn stimulates grazers such as ciliates, dinoflagellates and copepods. As phytoplankton blooms saturate the waters, the relative importance of grazers decreases and algal organic matter sediments into deeper waters. This promotes decomposition and aerobic respiration by both decomposers (Bacteria and Archaea) and bacterivore protists. Our data also support an important role of parasitism in C recycling and a tight coupling of NH_4^+ remineralization with its oxidation to NO_2^- by AOA (and less markedly to NO_3^- by NOB). Ammonia and NO_2^- oxidation are the only known aerobic links from the NH_4^+ produced by remineralization to the NO_x^- substrates of denitrification, which in anaerobiosis leads to N loss as N_2 and N_2O (Damashek & Francis 2018). Alternatively, NO_x^- may be effectively recycled to NH_4^+ by DNRA under anaerobic conditions. Wind patterns that cause intermittent mixing and ventilation of sub-pycnocline waters (O'Donnell et al. 2008) could also bring NO_3^- and NH_4^+ to depths with ideal light conditions, where these nutrients reinforce eutrophication (and thus hypoxia). While some pieces of this puzzle are regularly studied in estuaries with different DO levels, the complete dynamics (including the links between microbial plankton and geochemistry in both water and sediments) urgently needs clarification to predict feedbacks between water deoxygenation and greenhouse gas dynamics in these environments.

Authors' contributions. L.F.S. and G.B.M. conceived the study. L.F.S. and S.A.S. collected and processed DNA samples. D.I.G. collected and processed nutrient samples. L.F.S. led the project, analyzed the data and wrote the paper. All authors read, edited, and approved the paper.

Acknowledgements. We thank the Water Monitoring Program of the Connecticut Department of Energy and Environmental Protection (CT DEEP), especially Matthew Lyman and Katie O'Brien-Clayton, for allowing us to sample with them during 2 monitoring campaigns and for sharing environmental data. We also thank Kendra Maas (Microbial Analysis, Resources and Services facility, University of Connecticut) for sequencing, Craig Tobias (Department of Marine Sciences, University of Connecticut) for helpful discussions on estuarine nutrient dynamics, and 2 anonymous reviewers for constructive feedback. This work was funded by the University of Connecticut, including a Scholarship Facilitation Fund grant to L.F.S. L.F.S. and G.B.M. are also funded by a grant of the USA National Science Foundation (OCE-1924527).

LITERATURE CITED

Adl SM, Bass D, Lane CE, Lukeš J and others (2019) Revisions to the classification, nomenclature, and diversity of eukaryotes. J Eukaryot Microbiol 66:4–119

Ahlgren NA, Chen Y, Needham D, Parada AE and others (2017) Genome and epigenome of a novel marine *Thaumarchaeota* strain suggest viral infection, phosphorothioation DNA modification and multiple restriction systems. Environ Microbiol 19:2434–2452

Altenburger A, Blossom HE, Garcia-Cuetos L, Jakobsen HH and others (2020) Dimorphism in cryptophytes — the case of *Teleaulax amphioxeia/Plagioselmis prolonga* and its ecological implications. Sci Adv 6:eabb1611

Altieri AH, Gedan KB (2015) Climate change and dead zones. Glob Change Biol 21:1395–1406

Anderson TH, Taylor GT (2001) Nutrient pulses, plankton blooms, and seasonal hypoxia in western Long Island Sound. Estuaries 24:228–243

Apprill A, McNally S, Parsons R, Weber L (2015) Minor revision to V4 region SSU rRNA 806R gene primer greatly increases detection of SAR11 bacterioplankton. Aquat Microb Ecol 75:129–137

Auel H, Verheye HM (2007) Hypoxia tolerance in the copepod *Calanoides carinatus* and the effect of an intermediate oxygen minimum layer on copepod vertical distribution in the northern Benguela Current upwelling system and the Angola–Benguela Front. J Exp Mar Biol Ecol 352:234–243

Baird D, Christian RR, Peterson CH, Johnson GA (2004) Consequences of hypoxia on estuarine ecosystem function: energy diversion from consumers to microbes. Ecol Appl 14:805–822

Beaumont HJE, Hommes NG, Sayavedra-Soto LA, Arp DJ and others (2002) Nitrite reductase of *Nitrosomonas europaea* is not essential for production of gaseous nitrogen oxides and confers tolerance to nitrite. J Bacteriol 184:2557–2560

Beman JM, Carolan MT (2013) Deoxygenation alters bacterial diversity and community composition in the ocean's largest oxygen minimum zone. Nat Commun 4:2705

Bertagnolli AD, Stewart FJ (2018) Microbial niches in marine oxygen minimum zones. Nat Rev Microbiol 16:723–729

Bolyen E, Rideout JR, Dillon MR, Bokulich NA and others (2019) Reproducible, interactive, scalable and extensible microbiome data science using QIIME 2. Nat Biotechnol 37:852–857

Breitburg DL, Hondorp DW, Davias LA, Diaz RJ (2009) Hypoxia, nitrogen, and fisheries: integrating effects across local and global landscapes. Annu Rev Mar Sci 1:329–349

Breitburg D, Levin LA, Oschlies A, Grégoire M and others (2018) Declining oxygen in the global ocean and coastal waters. Science 359:eaam7240

Burki F, Roger AJ, Brown MW, Simpson AGB (2020) The new tree of eukaryotes. Trends Ecol Evol 35:43–55
Callahan BJ, McMurdie PJ, Rosen MJ, Han AW and others (2016) DADA2: high-resolution sample inference from Illumina amplicon data. Nat Methods 13:581–583
Capriulo GM, Smith G, Troy R, Wikfors GH and others (2002) The planktonic food web structure of a temperate zone estuary, and its alteration due to eutrophication. Hydrobiologia 475–476:263–333
Caron DA, Hutchins DA (2013) The effects of changing climate on microzooplankton grazing and community structure: drivers, predictions and knowledge gaps. J Plankton Res 35:235–252
Cavicchioli R, Ripple WJ, Timmis KN, Azam F and others (2019) Scientists' warning to humanity: microorganisms and climate change. Nat Rev Microbiol 17:569–586
Chambouvet A, Morin P, Marie D, Guillou L (2008) Control of toxic marine dinoflagellate blooms by serial parasitic killers. Science 322:1254–1257
Clarke KR (1993) Non-parametric multivariate analysis of changes in community structure. Aust J Ecol 18:117–143
Clarke KR, Ainsworth M (1993) A method of linking multivariate community structure to environmental variables. Mar Ecol Prog Ser 92:205–219
Coats DW, Heisler JJ (1989) Spatial and temporal occurrence of the parasitic dinoflagellate *Duboscquella cachoni* and its tintinnine host *Eutintinnus* pectinis in Chesapeake Bay. Mar Biol 101:401–409
Crump BC, Peranteau C, Beckingham B, Cornwell JC (2007) Respiratory succession and community succession of bacterioplankton in seasonally anoxic estuarine waters. Appl Environ Microbiol 73:6802–6810
CT DEEP (Connecticut Department of Energy and Environmental Protection) (2020) 2019 Long Island Sound hypoxia season review. https://portal.ct.gov/-/media/DEEP/water/lis_water_quality/hypoxia/FINAL_2019-Combined-Report_april2020.pdf?la=en (accessed 29 July 2021)
Damashek J, Francis CA (2018) Microbial nitrogen cycling in estuaries: from genes to ecosystem processes. Estuar Coasts 41:626–660
De La Iglesia R, Echenique-Subiabre I, Rodríguez-Marconi S, Espinoza JP and others (2020) Distinct oxygen environments shape picoeukaryote assemblages thriving oxygen minimum zone waters off central Chile. J Plankton Res 42:514–529
Diaz RJ, Rosenberg R (2008) Spreading dead zones and consequences for marine ecosystems. Science 321:926–929
Dolan JR, Coats DW (1991) Preliminary prey digestion in a predacious estuarine ciliate and the use of digestion data to estimate ingestion. Limnol Oceanogr 36:558–565
Douglas GM, Maffei VJ, Zaneveld JR, Yurgel S and others (2020) PICRUSt2 for prediction of metagenome functions. Nat Biotechnol 38:685–688
Edgcomb V, Orsi W, Bunge J, Jeon S and others (2011) Protistan microbial observatory in the Cariaco Basin, Caribbean. I. Pyrosequencing vs Sanger insights into species richness. ISME J 5:1344–1356
Eggleston EM, Lee DY, Owens MS, Cornwell JC and others (2015) Key respiratory genes elucidate bacterial community respiration in a seasonally anoxic estuary. Environ Microbiol 17:2306–2318
Ekau W, Auel H, Pörtner HO, Gilbert D (2010) Impacts of hypoxia on the structure and processes in pelagic communities (zooplankton, macro-invertebrates and fish). Biogeosciences 7:1669–1699
Elliott DT, Pierson JJ, Roman MR (2013) Copepods and hypoxia in Chesapeake Bay: abundance, vertical position and non-predatory mortality. J Plankton Res 35: 1027–1034
Fenchel T, Finlay BJ (1991) The biology of free-living anaerobic ciliates. Eur J Protistol 26:201–215
Fennel K, Testa JM (2019) Biogeochemical controls on coastal hypoxia. Annu Rev Mar Sci 11:105–130
Gobler CJ, Baumann H (2016) Hypoxia and acidification in ocean ecosystems: coupled dynamics and effects on marine life. Biol Lett 12:20150976
Gobler CJ, Berry DL, Dyhrman ST, Wilhelm SW and others (2011) Niche of harmful alga *Aureococcus anophagefferens* revealed through ecogenomics. Proc Natl Acad Sci USA 108:4352–4357
Godhantaraman N, Uye S (2003) Geographical and seasonal variations in taxonomic composition, abundance and biomass of microzooplankton across a brackish-water lagoonal system of Japan. J Plankton Res 25:465–482
Grasshoff KK, Kremling K, Ehrhardt M (1999) Methods of seawater analysis. Wiley-VCH, Weinheim
Guillou L, Bachar D, Audic S, Bass D and others (2013) The Protist Ribosomal Reference database (PR^2): a catalog of unicellular eukaryote small sub-unit rRNA sequences with curated taxonomy. Nucleic Acids Res 41:D597–D604
Hagy JD, Boynton WR, Keefe CW, Wood KV (2004) Hypoxia in Chesapeake Bay, 1950–2001: long-term change in relation to nutrient loading and river flow. Estuaries 27: 634–658
Hauss H, Christiansen S, Schütte F, Kiko R and others (2016) Dead zone or oasis in the open ocean? Zooplankton distribution and migration in low-oxygen modewater eddies. Biogeosciences 13:1977–1989
Helly JJ, Levin LA (2004) Global distribution of naturally occurring marine hypoxia on continental margins. Deep Sea Res I 51:1159–1168
Hewson I, Eggleston EM, Doherty M, Lee DY and others (2014) Metatranscriptomic analyses of plankton communities inhabiting surface and subpycnocline waters of the Chesapeake Bay during oxic-anoxic-oxic transitions. Appl Environ Microbiol 80:328–338
Hou L, Xie X, Wan X, Kao SJ and others (2018) Niche differentiation of ammonia and nitrite oxidizers along a salinity gradient from the Pearl River estuary to the South China Sea. Biogeosciences 15:5169–5187
Howarth R, Chan F, Conley DJ, Garnier J and others (2011) Coupled biogeochemical cycles: eutrophication and hypoxia in temperate estuaries and coastal marine ecosystems. Front Ecol Environ 9:18–26
Hutchins DA, Fu F (2017) Microorganisms and ocean global change. Nat Microbiol 2:17058
Kanehisa M, Sato Y (2020) KEGG Mapper for inferring cellular functions from protein sequences. Protein Sci 29:28–35
Keister JE, Tuttle LB (2013) Effects of bottom-layer hypoxia on spatial distributions and community structure of mesozooplankton in a sub-estuary of Puget Sound, Washington, USA. Limnol Oceanogr 58:667–680
Keister JE, Houde ED, Breitburg DL (2000) Effects of bottom-layer hypoxia on abundances and depth distributions of organisms in Patuxent River, Chesapeake Bay. Mar Ecol Prog Ser 205:43–59
Kemp WM, Boynton WR, Adolf JE, Boesch DF and others (2005) Eutrophication of Chesapeake Bay: historical trends and ecological interactions. Mar Ecol Prog Ser 303:1–29

Kozich JJ, Westcott SL, Baxter NT, Highlander SK and others (2013) Development of a dual-index sequencing strategy and curation pipeline for analyzing amplicon sequence data on the MiSeq Illumina sequencing platform. Appl Environ Microbiol 79:5112–5120

Kozlowski JA, Price J, Stein LY (2014) Revision of N_2O-producing pathways in the ammonia-oxidizing bacterium *Nitrosomonas europaea* ATCC 19718. Appl Environ Microbiol 80:4930–4935

Kuypers MM, Marchant HK, Kartal B (2018) The microbial nitrogen-cycling network. Nat Rev Microbiol 16:263–276

Lange V, Böhme I, Hofmann J, Lang K and others (2014) Cost-efficient high-throughput HLA typing by MiSeq amplicon sequencing. BMC Genomics 15:63

Legendre P, Legendre L (2012) Numerical ecology. Elsevier, Amsterdam

Lessard EJ (1991) The trophic role of heterotrophic dinoflagellates in diverse marine environments. Mar Microb Food Webs 5:49–58

López Abbate MC, Molinero JC, Guinder VA, Dutto MS and others (2015) Microplankton dynamics under heavy anthropogenic pressure. The case of the Bahía Blanca Estuary, southwestern Atlantic Ocean. Mar Pollut Bull 95:305–314

Löscher CR, Kock A, Könneke M, LaRoche J and others (2012) Production of oceanic nitrous oxide by ammonia-oxidizing archaea. Biogeosciences 9:2419–2429

Lücker S, Nowka B, Rattei T, Spieck E and others (2013) The genome of *Nitrospina gracilis* illuminates the metabolism and evolution of the major marine nitrite oxidizer. Front Microbiol 4:27

Ludsin SA, Zhang X, Brandt SB, Roman MR (2009) Hypoxia-avoidance by planktivorous fish in Chesapeake Bay: implications for food web interactions and fish recruitment. J Exp Mar Biol Ecol 381:S121–S131

Marcus NH, Richmond C, Sedlacek C, Miller G and others (2004) Impact of hypoxia on the survival and fecundity of *Acartia tonsa*. J Exp Mar Biol Ecol 301:111–128

Martin M (2011) Cutadapt removes adapter sequences from high-throughput sequencing reads. EMBnet J 17:10

Massana R, del Campo J, Sieracki M, Audic S and others (2014) Exploring the uncultured microeukaryote majority in the oceans: reevaluation of ribogroups within stramenopiles. ISME J 8:854–866

Naqvi S, Bange HW, Farías L, Monteiro PMS and others (2010) Marine hypoxia/anoxia as a source of CH_4 and N_2O. Biogeosciences 7:2159–2190

Ndhlovu A, Dhar N, Garg N, Xuma T and others (2017) A red tide forming dinoflagellate *Prorocentrum triestinum*: identification, phylogeny and impacts on St Helena Bay, South Africa. Phycologia 56:649–665

O'Donnell J, Dam HG, Bohlen WF, Fitzgerald W and others (2008) Intermittent ventilation in the hypoxic zone of western Long Island Sound during the summer of 2004. J Geophys Res Oceans 113:C09025

Oksanen J, Blanchet F, Friendly M, Kindt R and others (2019) vegan: community ecology package. R package version 2.5-6. https://CRAN.R-project.org/package=vegan (accessed 29 July 2021)

Parada AE, Needham DM, Fuhrman JA (2016) Every base matters: assessing small subunit rRNA primers for marine microbiomes with mock communities, time-series and global field samples. Environ Microbiol 18:1403–1414

Parsons RJ, Nelson CE, Carlson CA, Denman CC and others (2015) Marine bacterioplankton community turnover within seasonally hypoxic waters of a subtropical sound: Devil's Hole, Bermuda. Environ Microbiol 17: 3481–3499

Pedregosa F, Varoquaux G, Gramfort A, Michel V and others (2011) Scikit-learn: machine learning in Python. J Mach Learn Res 12:2825–2830

Prosser JI, Hink L, Gubry-Rangin C, Nicol GW (2020) Nitrous oxide production by ammonia oxidizers: physiological diversity, niche differentiation and potential mitigation strategies. Glob Change Biol 26:103–118

Putt M, Stoecker D (1989) An experimentally determined carbon:volume ratio for marine 'oligotrichous' ciliates from estuarine and coastal waters. Limnol Oceanogr 34: 1097–1103

Qin W, Heal KR, Ramdasi R, Kobelt JN and others (2017) *Nitrosopumilus maritimus* gen. nov., sp. nov., *Nitrosopumilus cobalaminigenes* sp. nov., *Nitrosopumilus oxyclinae* sp. nov., and *Nitrosopumilus ureiphilus* sp. nov., four marine ammonia-oxidizing archaea of the phylum *Thaumarchaeota*. Int J Syst Evol Microbiol 67:5067–5079

Quast C, Pruesse E, Yilmaz P, Gerken J and others (2013) The SILVA ribosomal RNA gene database project: improved data processing and web-based tools. Nucleic Acids Res 41:D590–D596

Quero GM, Celussi M, Relitti F, Kovačević V and others (2020) Inorganic and organic carbon uptake processes and their connection to microbial diversity in meso- and bathypelagic Arctic waters (Eastern Fram Strait). Microb Ecol 79:823–839

Rabouille C, Conley DJ, Dai MH, Cai WJ and others (2008) Comparison of hypoxia among four river-dominated ocean margins: the Changjiang (Yangtze), Mississippi, Pearl, and Rhône rivers. Cont Shelf Res 28:1527–1537

Ramond P, Sourisseau M, Simon N, Romac S and others (2019) Coupling between taxonomic and functional diversity in protistan coastal communities. Environ Microbiol 21:730–749

R Core Team (2020) A language and environment for statistical computing. R Foundation for Statistical Computing, Vienna. https://www.R-project.org

Reed M, Pinckney JL, Keppler CK, Brock LM and others (2016) The influence of nitrogen and phosphorus on seasonal phytoplankton growth and assemblage composition in four coastal, southeastern USA systems. Estuar Coast Shelf Sci 177:71–82

Ritchie GA, Nicholas DJ (1972) Identification of the sources of nitrous oxide produced by oxidative and reductive processes in *Nitrosomonas europaea*. Biochem J 126: 1181–1191

Roman M, Pierson JJ, Kimmel DG, Boicourt WC and others (2012) Impacts of hypoxia on zooplankton spatial distributions in the northern Gulf of Mexico. Estuar Coasts 35: 1261–1269

Santoferrara L (2019) Current practice in plankton metabarcoding: optimization and error management. J Plankton Res 41:571–582

Santoferrara L, Burki F, Filker S, Logares R and others (2020) Perspectives from ten years of protist studies by high-throughput metabarcoding. J Eukaryot Microbiol 67: 612–622

Santoro AE, Buchwald C, McIlvin MR, Casciotti KL (2011) Isotopic signature of N_2O produced by marine ammonia-oxidizing archaea. Science 333:1282–1285

Santoro AE, Richter RA, Dupont CL (2019) Planktonic marine archaea. Annu Rev Mar Sci 11:131–158

Schaefer SC, Hollibaugh JT (2017) Temperature decouples ammonium and nitrite oxidation in coastal waters. Environ Sci Technol 51:3157–3164

Schmidtko S, Stramma L, Visbeck M (2017) Decline in global oceanic oxygen content during the past five decades. Nature 542:335–339

Seibel BA, Schneider JL, Kaartvedt S, Wishner K and others (2016) Hypoxia tolerance and metabolic suppression in oxygen minimum zone euphausiids: implications for ocean deoxygenation and biogeochemical cycles. Integr Comp Biol 56:510–523

Skovgaard A (2014) Dirty tricks in the plankton: diversity and role of marine parasitic protists. Acta Protozool 53:51–62

Smith MW, Zeigler Allen L, Allen AE, Herfort L and others (2013) Contrasting genomic properties of free-living and particle-attached microbial assemblages within a coastal ecosystem. Front Microbiol 4:120

Spietz RL, Williams CM, Rocap G, Horner-Devine MC (2015) A dissolved oxygen threshold for shifts in bacterial community structure in a seasonally hypoxic estuary. PLOS ONE 10:e0135731

Stauffer BA, Schnetzer A, Gellene AG, Oberg C and others (2013) Effects of an acute hypoxic event on microplankton community structure in a coastal harbor of southern California. Estuar Coasts 36:135–148

Steckbauer A, Duarte CM, Carstensen J, Vaquer-Sunyer R and others (2011) Ecosystem impacts of hypoxia: thresholds of hypoxia and pathways to recovery. Environ Res Lett 6:025003

Stein LY, Arp DJ (1998) Loss of ammonia monooxygenase activity in *Nitrosomonas europaea* upon exposure to nitrite. Appl Environ Microbiol 64:4098–4102

Stoeck T, Bass D, Nebel M, Christen R and others (2010) Multiple marker parallel tag environmental DNA sequencing reveals a highly complex eukaryotic community in marine anoxic water. Mol Ecol 19:21–31

Stramma L, Johnson GC, Sprintall J, Mohrholz V (2008) Expanding oxygen-minimum zones in the tropical oceans. Science 320:655–658

Sun X, Kop LFM, Lau MCY, Frank J and others (2019) Uncultured *Nitrospina*-like species are major nitrite oxidizing bacteria in oxygen minimum zones. ISME J 13: 2391–2402

Tadonléké RD, Pollet T, Van Rijswijk P, Leberre B and others (2016) Effects of oxygen loss on carbon processing and heterotrophic prokaryotes from an estuarine ecosystem: results from stable isotope probing and cytometry analyses. Estuar Coasts 39:992–1005

Tolar BB, King GM, Hollibaugh JT (2013) An analysis of Thaumarchaeota populations from the northern Gulf of Mexico. Front Microbiol 4:72

Torres-Beltrán M, Sehein T, Pachiadaki MG, Hallam SJ, Edgcomb V (2018) Protistan parasites along oxygen gradients in a seasonally anoxic fjord: a network approach to assessing potential host-parasite interactions. Deep Sea Res II 156:97–110

Trimmer M, Chronopoulou PM, Maanoja ST, Upstill-Goddard R and others (2016) Nitrous oxide as a function of oxygen and archaeal gene abundance in the North Pacific. Nat Commun 7:13451

Valdés V, Carlotti F, Escribano R, Donoso K and others (2018) Nitrogen and phosphorus recycling mediated by copepods and response of bacterioplankton community from three contrasting areas in the western tropical South Pacific (20° S). Biogeosciences 15:6019–6032

Vaquer-Sunyer R, Duarte C (2008) Thresholds of hypoxia for marine biodiversity. Proc Natl Acad Sci USA 105: 15452–15457

Verity PG, Borkman DG (2010) A decade of change in the Skidaway River Estuary. III. Plankton. Estuar Coast 33: 513–540

Voss M, Bange HW, Dippner JW, Middelburg JJ and others (2013) The marine nitrogen cycle: recent discoveries, uncertainties and the potential relevance of climate change. Philos Trans R Soc B 368:20130121

Walker CB, de la Torre JR, Klotz MG, Urakawa H and others (2010) *Nitrosopumilus maritimus* genome reveals unique mechanisms for nitrification and autotrophy in globally distributed marine crenarchaea. Proc Natl Acad Sci USA 107:8818–8823

Ward BB (2013) How nitrogen is lost. Science 341:352–353

Ward CS, Yung CM, Davis KM, Blinebry SK and others (2017) Annual community patterns are driven by seasonal switching between closely related marine bacteria. ISME J 11:1412–1422

Welschmeyer NA (1994) Fluorometric analysis of chlorophyll *a* in the presence of chlorophyll *b* and phaeopigments. Limnol Oceanogr 39:1985–1992

Whitney MM, Vlahos P (2021) Reducing hypoxia in an urban estuary despite climate warning. Environ Sci Technol 55:941–951

Wilson RE, Swanson RL, Crowley HA (2008) Perspectives on long-term variations in hypoxic conditions in western Long Island Sound. J Geophys Res Oceans 113:C12011

Wrage-Mönnig N, Horn MA, Well R, Müller C and others (2018) The role of nitrifier denitrification in the production of nitrous oxide revisited. Soil Biol Biochem 123:A3–A16

Wright JJ, Konwar K, Hallam S (2012) Microbial ecology of expanding oxygen minimum zones. Nat Rev Microbiol 10:381–394

Wu DM, Dai QP, Liu XZ, Fan YP and others (2019) Comparison of bacterial community structure and potential functions in hypoxic and non-hypoxic zones of the Changjiang Estuary. PLOS ONE 14:e0217431

Ye Q, Wu Y, Zhu Z, Wang X and others (2016) Bacterial diversity in the surface sediments of the hypoxic zone near the Changjiang Estuary and in the East China Sea. MicrobiologyOpen 5:323–339

Zhang J, Gilbert D, Gooday AJ, Levin L and others (2010) Natural and human-induced hypoxia and consequences for coastal areas: synthesis and future development. Biogeosciences 7:1443–1467

Zhu X, Burger M, Doane TA, Horwath WR (2013) Ammonia oxidation pathways and nitrifier denitrification are significant sources of N_2O and NO under low oxygen availability. Proc Natl Acad Sci USA 110:6328–6333

Zhu-Barker X, Cavazos AR, Ostrom NE, Horwath WR and others (2015) The importance of abiotic reactions for nitrous oxide production. Biogeochemistry 126:251–267

Zimmerman CF, Keefe CW (1991) EPA Method 353.4., Determination of nitrite and nitrate in estuarine and coastal waters by automated colorimetric analysis In: An interim manual of methods for the determination of nutrients in estuarine and coastal waters. Rev 1.1. US EPA

Zou D, Liu H, Li M (2020) Community, distribution, and ecological roles of estuarine Archaea. Front Microbiol 11:2060

Appendix.

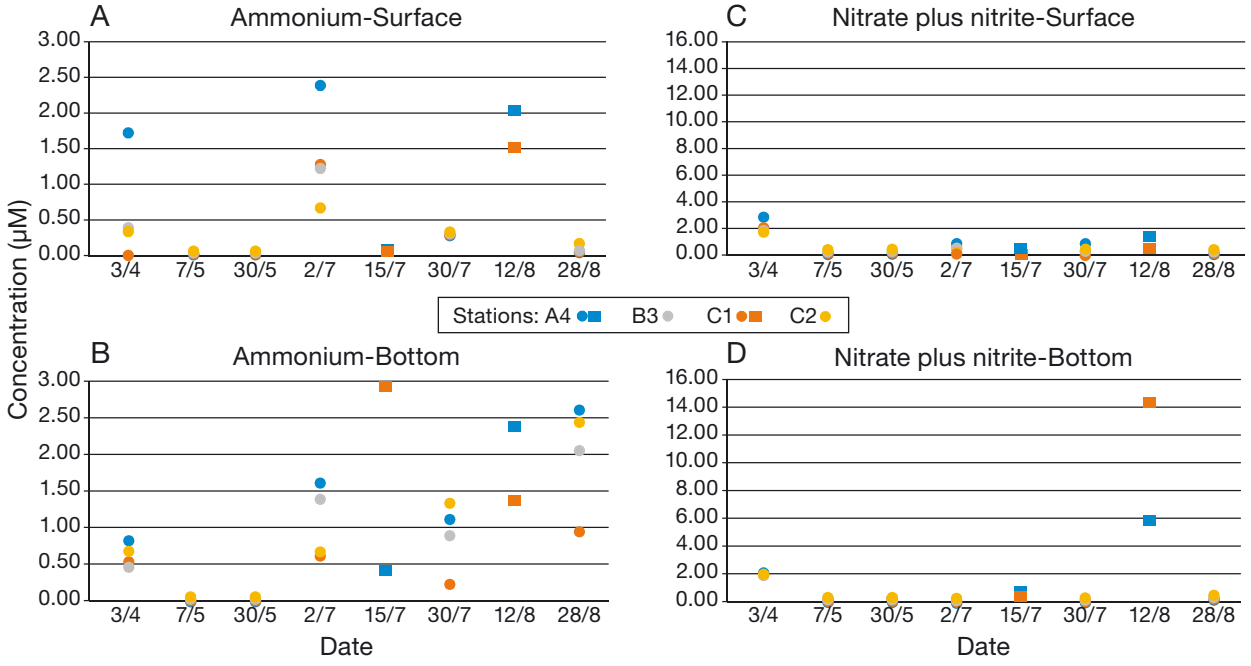

Fig. A1. Concentrations of (A,B) ammonium and (C,D) nitrate plus nitrite in (A,C) surface and (B,D) bottom waters of western Long Island Sound during summer 2019. Quantifications by the Connecticut Department of Energy and Environmental Protection (circles) and the present study (squares). Dates are dd/mm

Editorial responsibility: Klaus Jürgens, Rostock, Germany
Reviewed by: E. A Suter, C. Loescher

Submitted: July 29, 2021
Accepted: November 22, 2021
Proofs received from author(s): February 17, 2022